Effect of specimen geometries on the C⋆ versus da/dt master curve for type 316L stainless steel

Lucien Laiarinandrasana, Moulay Rachid Kabiri, Magali Reytier

Effect of specimen geometries on the C^* versus da/dt master curve for type 316L stainless steel

L. Laiarinandrasana [a,*], M.R. Kabiri [b], M. Reytier [c]

[a] *Centre des Matériaux, Ecole des Mines de Paris, UMR CNRS 7633, BP 87, 91003 Evry Cedex, France*
[b] *Ecole Nationale Supérieure d'Arts et Métiers, BP4024 Béni M'Hamed, Morocco*
[c] *CEA Saclay, 91191 Gif-sur-Yvette Cedex, France*

This work deals with engineering components made of stainless steels working at high temperature and subjected to creep-fatigue loading history. The defect assessment procedures generally use the crack growth properties curve da/dt versus C^* parameter for estimating the creep-crack growth. The ASTM E 1457-98 [ASTM E 1457-98. Standard test method for measurement of creep crack growth rates in metals, 1998] procedure proposes the rule to establish such a master curve. In particular, it is stipulated that this rule only applies for CT specimens. Previously [Laiarinandrasana L, Kabiri R, Drubay B. In: Gupta A, editor. Proceedings of the 16th international conference on structural mechanics in reactor technology, Washington, USA, 2001], some practical methodology to produce this crack growth curve on CT specimens has been described by introducing the way to determine the upper and lower limits of relevant experimental points and by adopting the ASTM E 1457-98 method to estimate the creep component of the load line displacement rate ($\mathrm{d}\delta/\mathrm{d}t_{\mathrm{behavior}}$). This latter is the interesting part of the total displacement rate recorded during the test. This paper focuses on the application of the procedure proposed in [Laiarinandrasana L, Kabiri R, Drubay B. In: Gupta A, editor. Proceedings of the 16th international conference on structural mechanics in reactor technology, Washington, USA, 2001] on specimen geometries other than CT, such as circumferentially cracked round bar (CCRB) and double edged notched in tension (DENT) specimens. The da/dt versus C^* curves issued from all of these specimens are compared. Discussion about the effect of geometry on these curves is carried out. Additionally, some finite element analyses have been performed in order to simulate the creep crack growth using the node release technique. These simulations allow to verify the validity of the proposed expressions of C^* and consequently the master curve of the 316L(N) stainless steel.

1. Introduction

High temperature structural components are often subjected to non-uniform stress and temperature distribution during service. These conditions may favour localized creep damage in the form of service initiated

* Corresponding author. Tel.: +33 1 60 76 30 64; fax: +33 1 60 76 31 60.
E-mail address: lucien.laiarinandrasana@ensmp.fr (L. Laiarinandrasana).

Nomenclature

A	crack growth material parameter
a	crack depth (mm)
$\dot{a}$	crack growth rate (mm/h)
B	plane specimens thickness (mm)
B_0, B_1, B_2	plastic, primary creep and secondary creep material parameters
E	Young's modulus
J_P	fully plastic component of the J-integral calculated using EPRI method
K_I	the stress intensity factor
n, n_1, n_2	plastic, primary creep and secondary creep stress exponents
P	applied load (N)
p_1	primary creep time exponents
q	crack growth correlation C^* exponent
t	time (h)
W	plane specimens width (mm)
δ, $\dot{\delta}$	load line displacement, load line displacement rate
σ_{ref}	reference stress

cracks which can propagate and ultimately cause fracture. A significant portion of the component life can, however, be spent in crack propagation. Therefore, there is considerable interest in developing the technology for predicting creep crack growth behavior.

The ASTM E 1457-98 [1] procedure proposes the rule to establish a master curve relating the creep crack growth rate (da/dt) to the fracture mechanics load parameter C^*. Throughout this paper the crack growth properties curve related to da/dt versus C^* parameter will be referred to as master curve. In [2] some recommendations concerning the construction of the da/dt versus C^* master curve applied on CT specimens have been suggested. In the present paper, an attempt is made to generalize this procedure to other specimens such as circumferentially cracked round bar (CCRB) and double edged notched in tension (DENT) specimens, in order to show the relevance of the master curve of type 316L stainless steel.

At first, the characteristics of materials and specimens which this study deals with are presented, then analytical expressions to calculate the supposed "experimental" load parameter C^* for each specimen are introduced. Recommendations in Ref. [2] have been followed especially concerning the domain of validity of the experimental points in order to plot 316L(N) master curve. At last, the validation of the proposed procedure by a finite element (FE) method simulating creep crack growth with node release technique is carried out.

2. Experimental data

The creep tests were carried out at the Ecole des Mines de Paris (Piques, 1989) and (Maas, 1986) on the "SQ" sheet, Imperial College on the "SD" sheet, and CEA-SACLAY on "VIRGO" sheet of the 316L stainless steel. Constant loads have been applied during the tests at 550, 575, 600, and 650 °C.

The chemical compositions of the materials are given in Table 1, whereas Table 2 summarizes the conventional tensile properties of all sheets at the prescribed temperatures.

Table 1
Chemical compositions of all sheets (wt.%)

Sheet	C	Mn	Si	S	P	Ni	Cr	Mo	N	Cu	Co	B
SQ	0.028	1.88	0.3	0.001	0.028	12.46	17.31	2.44	0.077	0.175	0.135	0.0012
SD	0.038	1.83	0.313	0.02	0.036	11.9	17.3	2.46	0.067	0.27	–	–
VIRGO	0.022	1.8	0.38	0.02	0.021	13.3	17	2.25	0.032	0.032	–	0.0014

Table 2
Tensile properties of all sheets of 316L stainless steel

Sheet	Temperature (°C)	Elastic modulus (MPa)	Yield strength (MPa)	Tensile strength (MPa)
SQ	575	144,000	149	428
	600	144,000	146	407
	650	144,000	141	367
SD	650	148,000	167	403
VIRGO	550	144,000	112	361

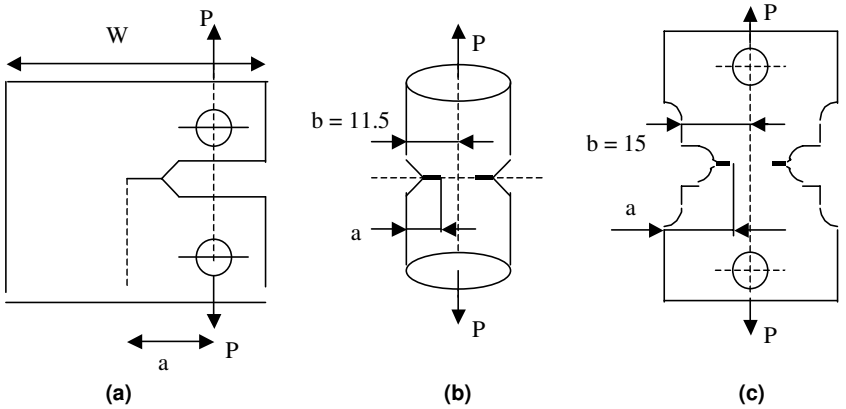

Fig. 1. Specimens geometries: (a) CT; (b) CCRB; (c) DENT.

In order to verify the specimen effect on da/dt versus C^* master curve, three specimen geometries have been analysed: compact tension (CT), circumferentially cracked round bar (CCRB), and double edge notch tensile (DENT). These specimens were fatigue precracked at room temperature. They were instrumented to measure both the load line displacement $\delta(t)$, and the crack length $a(t)$ during the creep tests. More details on the specimens geometries are reported in Fig. 1. The characteristic dimensions of EMPs CT specimen (4CT) are: $W = 40$ mm, $B = 10$ mm, those of Imperial College (3CT) are $W = 50$, $B = 23.8$ mm and $W = 25$ mm, $B = 12.7$ mm, and those of CEA (2CT) are side-grooved, $W = 50$ mm, $B_{\text{total}} = 25$ mm, $B_{\text{net}} = 20$ mm. Experimental data for all specimens consist of files containing the time, the load-line displacement and the crack depth. For EMPs CT and CCRB specimens, data are available in [3].

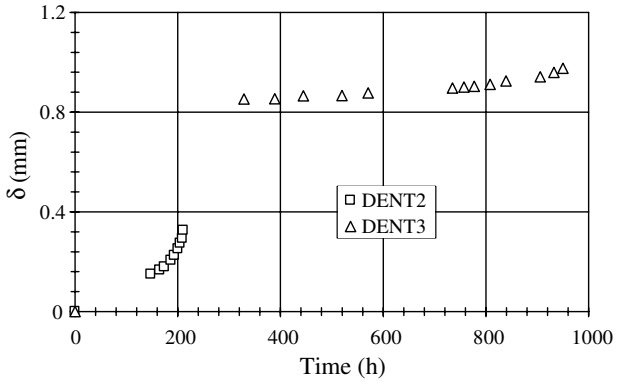

Fig. 2. Creep tests of DENT specimens.

Table 3
Values of plasticity and creep laws coefficients

Sheet	Temperature (°C)	B_0 (MPa^{-n})	n	B_1 ($MPa^{-n_1}\ h^{-p_1}$)	n_1	p_1	B_2 ($MPa^{-n_2}\ h^{-1}$)	n_2
SQ	575	–	–	9×10^{-14}	4	0.43	–	–
	600	2.86×10^{-8}	2.4968	1.441×10^{-14}	4.642	0.5135	1.6325×10^{-25}	7.69
	650	–	–	2.633×10^{-14}	4.7463	0.57	6.95×10^{-25}	7.69
SD	650	3.838×10^{-25}	2.872	5.863×10^{-13}	4.233	0.565	1.018×10^{-25}	9.407
VIRGO	550	–	–	4.414×10^{-12}	3.361	0.411	6.71×10^{-24}	8.4

By comparing measured crack mouth opening displacement history with simulation results by using finite element (FE) investigations [4], it turned out that CT specimens experimental points were nearer to FE simulation under plane strain conditions whereas DENT data were close to plane stress analyses. It should be remembered that for 2D modelling, conversely to CT and DENT, CCRB is an interesting specimen in the sense that they need neither plane strain nor plane stress conditions.

In the authors knowledge, there are scarcely available experimental data for specimen types other than CT and CCRB, apart from 2 DENT issued from [5]. Unfortunately, they are not complete as it can be seen in Fig. 2. Nonetheless, those tests will be utilized here and analysed under plane stress conditions [5]. It should be mentioned that European CRETE project [6] test programme consisted of performing creep crack growth tests on seven (7) types of cracked specimens. This would bring a better understanding of the geometry effects once the data are analysed.

3. Creep behavior

Prior to creep behavior, the tensile stress–strain plastic law is supposed to be described by

$$\varepsilon = B_0\sigma^n \tag{1}$$

For the time-dependent constitutive relationship of 316L stainless steel, both primary and secondary creep behaviors have been taken into account with standard power creep laws described as follows:

$$\text{Primary creep:}\quad \varepsilon = B_1\sigma^{n_1}t^{p_1} \tag{2}$$

$$\text{Secondary creep:}\quad \dot{\varepsilon} = B_2\sigma^{n_2} \tag{3}$$

The values of different material coefficients of plasticity and creep laws are given, for each sheet in Table 3.

4. Determination of C^*

The load parameter C^* is calculated from the load-line displacement rate $\mathrm{d}\delta_{\exp}/\mathrm{d}t = \dot{\delta}_{\exp}$ which is supposed to split into a part due to the creep behavior noted $\dot{\delta}_C$ and a part due to the structure response related to the crack growth noted $\dot{\delta}_S$:

$$\dot{\delta}_{\exp} = \dot{\delta}_C + \dot{\delta}_S \tag{4}$$

For each specimen type, C^* parameter is calculated using only the part of the load-line displacement rate due to the creep behavior. It is assumed that the structural term $\dot{\delta}_S$ is uniquely due to the crack advance (elastic–plastic term, not time dependent) and may be estimated [7–9]. Note that this load-line displacement is directly related to J-integral. It is then easy to deduce this term as follows:

$$\text{For CT [1] and DENT specimens:}\quad \dot{\delta}_C = \dot{\delta}_{\exp} - \frac{\dot{a}B}{P}\left[\frac{2K_I^2}{E^*} + (n+1)J_P^{\mathrm{EPRI}}\right] \tag{5}$$

$$\text{For CCRB specimen:}\quad \dot{\delta}_C = \dot{\delta}_{\exp} - \frac{2\pi\dot{a}b}{P}\left[\frac{2K_I^2}{E} + (n+1)J_P^{\mathrm{EMP}}\right] \tag{6}$$

where $J_P^{\mathrm{EMP}} = \frac{n-1}{n+1}\frac{P\delta}{2\pi(b-a)^2}$ according to [3].

It should be mentioned that Ref. [7] method does not provide J_P formulation for CCRB specimens. Additionally, only Eq. (5) requires the stress state as plane stress or plane strain conditions. Thus, we can formulate the load parameter C^* for each specimen type as follows [4]:

$$\text{For the CT specimens [1–4,13,14]: } C^*(\text{CT}) = \left[2 + 0.522\left(1 - \frac{a}{W}\right)\right] \frac{n_2}{n_2 + 1} \frac{P\dot{\delta}_C}{B(W - a)} \tag{7}$$

$$\text{For the CCRB specimens [3,4,13]: } C^* = \frac{n_2 - 1}{n_2 + 1} \frac{P\dot{\delta}_C}{2\pi(b - a)^2} \tag{8}$$

$$\text{For the DENT specimens [3,4,14]: } C^* = \frac{1}{2} \frac{n_2 - 1}{n_2 + 1} \frac{P\dot{\delta}_C}{B(b - a)} \tag{9}$$

Since Eqs. (7)–(9) use experimental values of $\dot{\delta}_C$, the stress state (plane stress/strain) does not directly interfere.

5. Domain of validity of the d*a*/d*t* versus *C** correlation

In [2] it has been assumed that the lower limit of the $\dot{a}$ versus C^* curve corresponds to the starting point of the last transient stage of creep. For 316L(N) stainless steel, this point coincides to the C^* minimum value.

Concerning the upper bound, the ASTM E1457 procedure has not been applied since $\dot{\delta}_C$ is supposed to be well estimated throughout the test. Thus, it is suggested [3] that the upper limit is representative of the time when $\dot{\delta}_C$ deviates from the secondary creep stage. To do this, the reference length concept [3] is used. The secondary creep regime is established as long as $\dot{\delta}_C$ is proportional to $(W - a)B_2\sigma_{\text{ref}}^{n_2}$, where σ_{ref} is the reference stress of the specimen given according to [7,8]. In the following, only experimental points corresponding to these descriptions will be selected.

6. The master curve of 316L(N)

6.1. da/dt versus C correlation of "SQ" sheet*

Creep tests performed at the Ecole des Mines de Paris are first addressed (4 CT, 14 CCRB and 2 DENT). da/dt versus C^* curve is plotted for each specimen type. Results in Fig. 3 shows that there is a unique correlation for each specimen.

By merging the results illustrated in Fig. 3 into a unique da/dt versus C^* curve, all of the experimental points of the three specimens are utilized in order to fit a power law $\mathrm{d}a/\mathrm{d}t = AC^{*q}$.

Fig. 4 shows that, within a scatter band of about factor 2, a unique correlation is obtained for 3 specimen geometries and 3 temperature tests ranging from 550 °C to 650 °C. By fitting coefficients A and q of the $\mathrm{d}a/\mathrm{d}t = AC^{*q}$ (see Table 4) it comes out that they are very close to the values given earlier by Laiarinandrasana et al. [2] on CT specimen type alone. So, for the "SQ" sheet, it can be concluded that there is no effect of specimen geometries on the da/dt versus C^* curve.

6.2. da/dt versus C correlation of "SD" and "VIRGO" sheets*

Fig. 5(a) displays the results for the "SD" sheet of the 316L(N) tests where a correlation da/dt versus C^* load parameter is depicted. In Fig. 5(b), a unique correlation da/dt versus C^* characterizes the creep crack growth in the "VIRGO" sheet.

6.3. Master curve of the 316L(N) stainless steel

All of previous da/dt versus C^* curves are now gathered into the same diagram (Fig. 6) allowing to show the results for the 316L(N) stainless steel tests. Experimental points corresponding to three sheets are represented is the same figure. The adjusted coefficients ($A = 0.016$, $q = 0.7$) are the same as those established on the "SQ" sheet. The same result has been reported [3] by using the reference length concept.

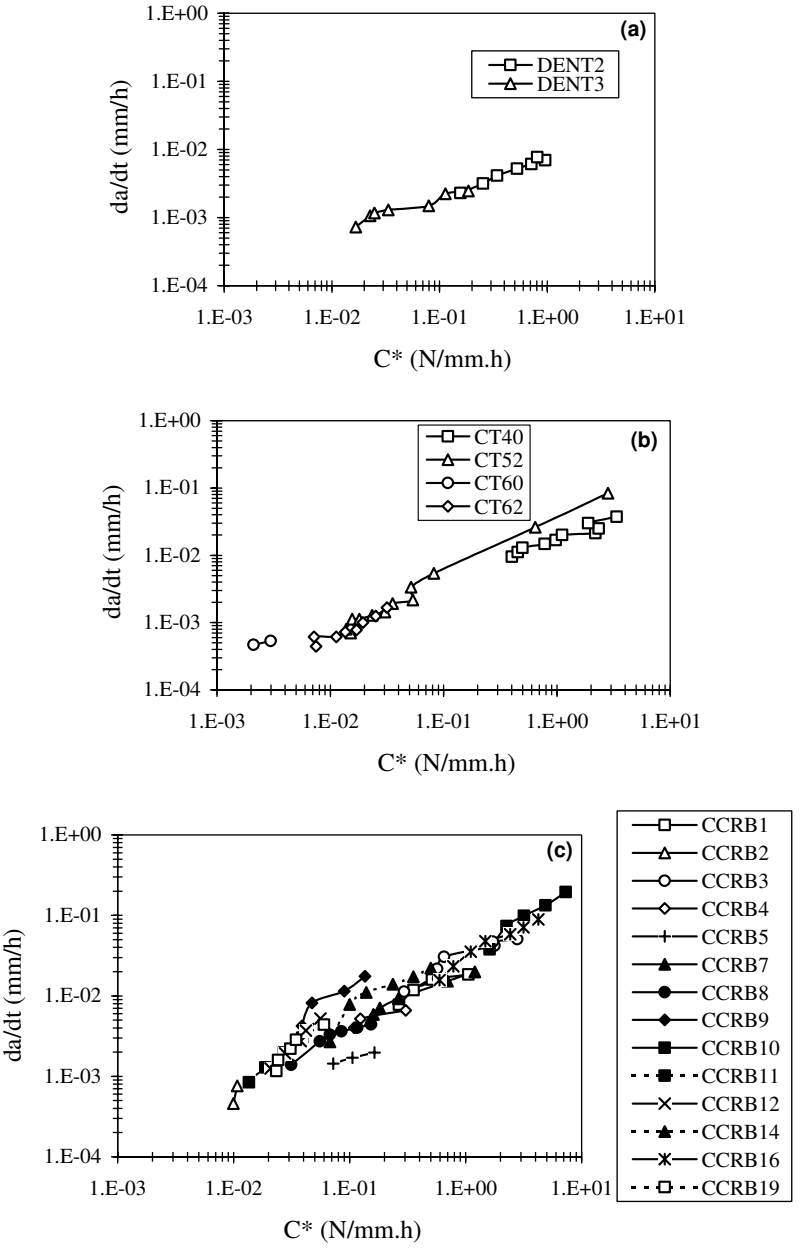

Fig. 3. da/dt versus C^* curve for each specimens type: (a) DENT, (b) CT and (c) CCRB.

7. Finite element simulations

This section aims at estimating numerically the crack mouth opening displacement rate history for a propagating crack. Hence, the crack growth is not simulated but imposed as a boundary condition in the FE analysis. In other words, the crack mouth opening displacement is a result of the investigation. Its history is to be compared with the experimental data. To achieve this goal, FE computations with node release technique [10] have been carried out [11] on 9 specimens (CCRB (5), DENT (1), CT (3)). A worked example is described below with a CCRB specimen denoted as CCRB1, tested at 600 °C with $P = 52630N$. The characteristic

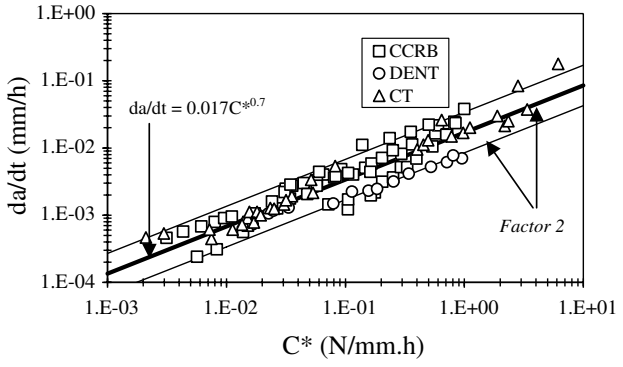

Fig. 4. da/dt versus C^* curve for "SQ" sheet of 316L(N)—all specimens.

Table 4
Values of coefficients in da/d$t = AC^{*q}$ correlation

	A (N^{-q} mm^{q+1} h^{q-1})	q
Present work	0.017	0.7
In Ref. [2]	0.016	0.71

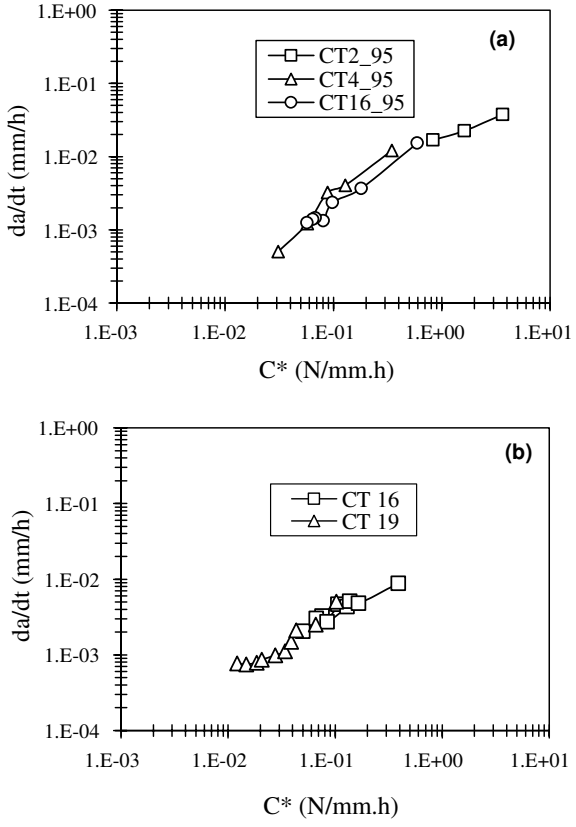

Fig. 5. da/dt versus C^* curve for CT specimens type: (a) "SD" sheet and (b) "VIRGO" sheet.

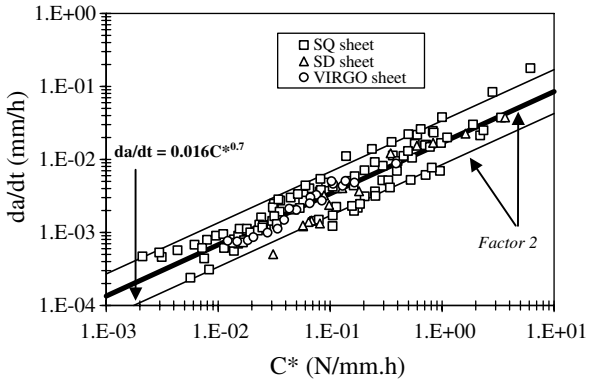

Fig. 6. da/dt versus C^* master curve of the 316L(N) stainless steel.

dimensions are: nominal radius $b = 11.5$ mm, initial crack depth ratio $a_0/b = 0.45$. The crack incubation time is 25 h and the crack growth is illustrated in Fig. 7.

The FE computation uses 2D axi-symmetric iso-parametric elements with reduced integration. Only half of the geometry is meshed. The load is applied to the node set at the top of the mesh whereas the crack growth is numerically imposed by gradually releasing the nodes (12 steps) in the remaining ligament following $a(t)$ in Fig. 7. The constitutive equations are based on double inelastic deformation (DID) approach [12], allowing to separate the plastic and visco-plastic strains.

Initial and deformed meshes (at the end of the crack growth simulation) are depicted in Fig. 8. As a result, both simulated and experimental total load-line displacement histories are plotted in Fig. 9. Since consecutive nodes are released in a discrete way, the simulated curve shows a stepwise trend. Although a scatter is depicted in Fig. 9 between simulated and experimental values, the key point here is the load-line displacement rates. Qualitatively, these latter seem to be in agreement. In order to compare the order of magnitude of the load-line displacement rates, the above mentioned simulated curve has been smoothed. In Fig. 10 the obtained plot is labelled as "propagating crack". This plot is the starting point to extract the numerical creep component of the load-line displacement. Then, several FE analyses of the same specimen but with various constant crack depth ratios have been carried out. For a given value of a/b, ranging from a_0/b to $(a_0 + 550\ \mu\text{m})/b$, simulations are performed up to the time when the propagating crack reaches the actual a/b. In Fig. 10, the dashed line corresponds to the simulation of a stationary crack at $a = a_0 + 300\ \mu$m. This crack advance of 300 μm is reached at time $t = 143.3$ h, hence the simulation of stationary crack corresponding to $(a_0 + 300\ \mu\text{m})$ is performed up to $t = 143.3$ h. At this time, the total amount of the crack mouth opening displacement is 231 μm whereas the corresponding numerical value obtained on stationary crack is: $\delta_C = 185\ \mu$m.

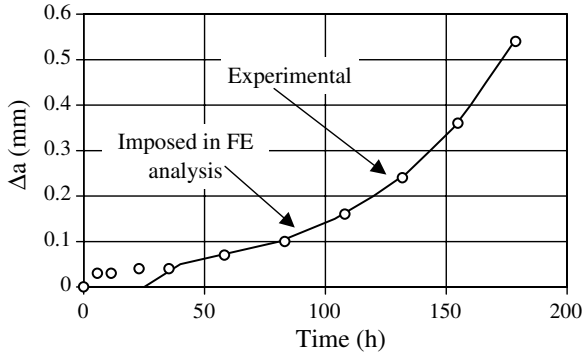

Fig. 7. Crack growth curves for CCRB1 specimen.

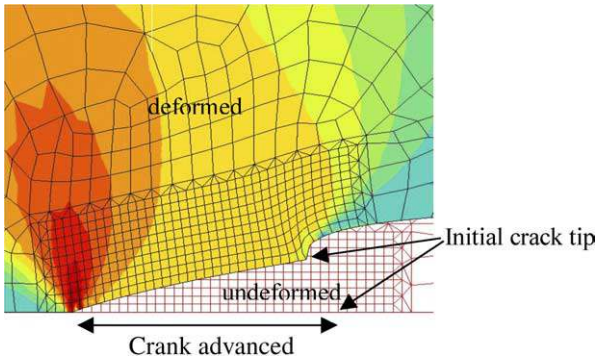

Fig. 8. Deformed and undeformed meshes in the vicinity of the crack tip.

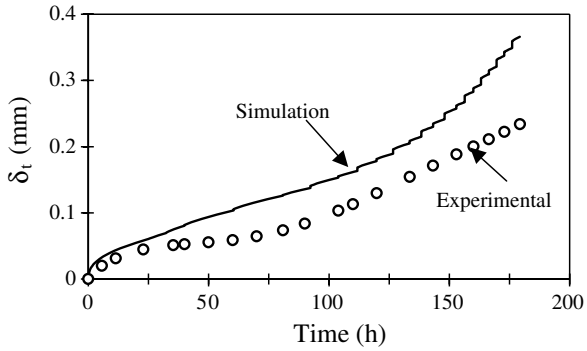

Fig. 9. Comparison between experimental and simulated total load-line displacement (CCRB1).

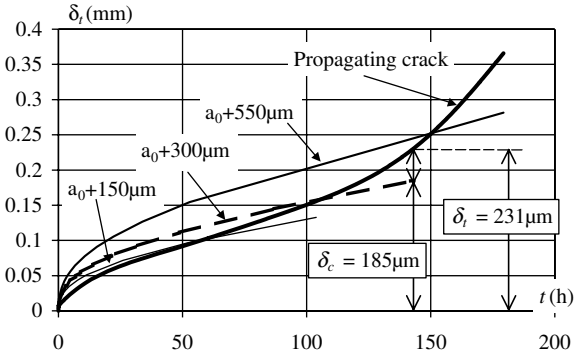

Fig. 10. Determination of numerical δ_C.

The remainder is identified as the structural component due to the crack advance: $\delta_S = 46$ μm. Conversely to the ASTM procedure [1], this methodology enables to directly estimate δ_C.

From the curves plotted in Fig. 10, the displacement rates are calculated. The results are illustrated in Fig. 11 where we have limited the plot within the validation time range. Open symbols refer to results deduced from FE analysis whereas full symbols correspond to exploitation of the experimental data. So, starting from "total experimental" curve (full squares), the elastic–plastic contribution is calculated following ASTM recommendation [1], leading to the curve labelled "Structure ASTM" (full circles). The required creep component of displacement rate is deduced via Eq. (5), giving the curve labelled "Creep ASTM" (full triangles).

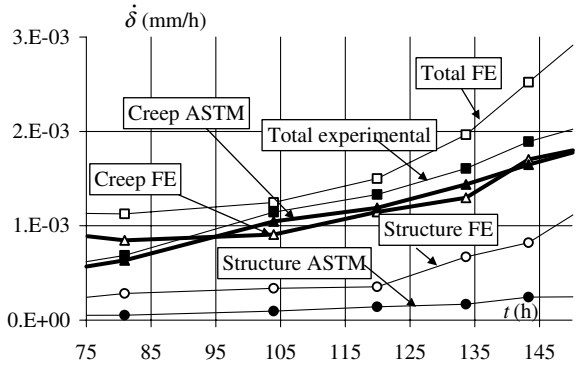

Fig. 11. Displacement rate partitioning, CCRB1.

For the simulated quantities, "Total FE" (open squares) is the initial curve, then "Creep FE" (open triangles) is obtained by using the aforementioned procedure (see Fig. 10) and "Structure FE" (open circles) stands for the structural term due to the crack advance by subtraction of "Creep FE" from "Total FE".

Fig. 11 clearly shows that there is excellent agreement between "Creep ASTM" and "Creep FE". The same trends have been observed for all round bars simulated tests. For plane geometries such as DENT and CT specimens the stress state hypotheses (PE or PS) induce a larger scatter than for round bars.

Some comments should be added concerning C^* calculations. The numerical integration of the C^* parameter utilizes the creep strain rate (hence creep displacement rate). It has been reported [4] that the values of C^* given by numerical calculations and by Eqs. (7)–(9), respectively, are in good agreement. Additionally, by

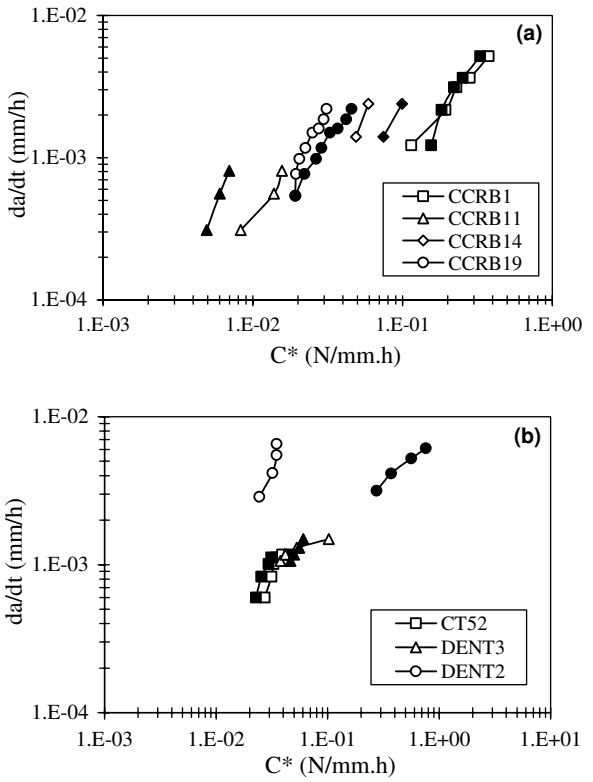

Fig. 12. Comparison between experiment and simulation. (a) CCRB; (b) CT and DENT.

using creep displacement rate value given by ASTM in Eqs. (7)–(9), C^* values are found to be similar. In conclusion, numerical C^* values calculated for a propagating crack coincide well with the ASTM method based on the displacement rate partitioning.

In Fig. 12, comparisons are made between selected "experimental" curves issued from Fig. 6 and their computed counterparts. Note that da/dt scale has been changed (ranging from 10^{-4} mm/h to 10^{-2} mm/h) in order to enhance the difference in the comparison. In the following comments, full symbols deal with simulated value whereas empty ones will refer to experiments. In Fig. 12(a) the CCRB1 curves (square symbols) indicate an excellent agreement between experimental and numerical simulations. For CCRB11 (triangle symbols) and CCRB14 (diamond symbols), the shift between experimental/simulated curves is uniquely due to $\dot{\delta}_C$ difference. This can be proved from Eq. (8).

Fig. 12(b) shows again the accordance between numerical simulation and experimental curve for CT52 (square symbols) and DENT3 (triangle symbols). For this latter case, although the experimental data is incomplete, a portion of stationary creep stage seems to appear (see Fig. 2). The good agreement between simulation and experiment for DENT3 means that the experimental $\dot{\delta}_C$ is well represented by the strain rate obtained from the constitutive equation (DID model). That is not the case for DENT2 specimen. In Fig. 2, only the end of the experimental curve is available. In order to calculate a correct C^* value, an interpolation of $\dot{\delta}_C$ is needed. However, it should be noted that the experimental values are in the same trend as for other specimens.

Finally, the node release technique used to simulate the creep crack mouth opening displacement history under propagating crack provides excellent results. C^* formulae in Eqs. (7)–(9) give the same estimates either with ASTM $\dot{\delta}_C$ or with FE $\dot{\delta}_C$. These C^* values are also in accordance with the FE computed C^*. Hence, Fig. 6 can be reproduced by using finite element C^* values. This allows to extend the use of the master curve to cracked bodies that are not provided with C^* formula.

8. Conclusion

The ASTM E 1459-98 standard [1] covers the determination of creep crack growth on CT specimens at high temperature on a creep ductile materials when the use of C^* load parameter is relevant. This procedure can be extended to other types of specimen. In the case of 316L(N) stainless steel, three specimens (CT, CCRB, and DENT) were tested at various temperatures (550, 575, 600, and 650 °C). In order to characterize the creep crack growth of this material, the part due to crack growth has been extracted from the load line displacement rate. Formulae allowing to calculate C^* for CCRB and DENT specimens have been proposed. In addition, limits of the domain of investigation have been discussed. Especially, the upper bound is characterized by using the reference length concept.

Creep crack growth on 27 specimens of three sheets (SQ, SD and VIRGO) were analysed. For each test the same procedure has been employed. Finite element simulations on 12 specimens were carried out at 600 °C using the node release technique. These investigations show that a unique master curve da/dt versus C^* can be described for 316L(N) stainless steel. No effect of geometry (CCRB, CT and DENT) seems to be observed over a large temperature range (from 550 °C to 650 °C) and for a crack depth ratios covering 0.42 to 0.69. The correlation coefficients according to $da/dt = AC^{*q}$ are: $A = 0.016$, $q = 0.7$.

References

[1] ASTM E 1457-98. Standard test method for measurement of creep crack growth rates in metals, 1998.

[2] Laiarinandrasana L, Kabiri R, Drubay B. In: Gupta A, editor. Proceedings of the 16th international conference on structural mechanics in reactor technology, Washington, USA, 2001.

[3] Piques R. Mechanics and mechanisms to crack initiation and growth under viscoplastic conditions in an austenitic stainless steel. Thesis, Ecole Nationale Supérieure des Mines de Paris, 1989 [in French].

[4] Kabiri MR. High temperature cracking of steels: effects of geometry on creep crack growth laws. Thesis, Ecole Nationale Supérieure des Mines de Paris, 2003 [in French].

[5] Maas E. Creep crack growth in the austenitic stainless steel Z3-CND17-13. Thesis, Ecole Nationale Supérieure des Mines de Paris, 1989 [in French].

[6] CRETE. Development and harmonisation of creep crack growth testing for industrial specimens: a route to a European Code Practice. CORDIS RTD-PROJECTS (European Communities), Record Control Number: 55425, 1994. Available from: http://dbs.cordis.lu/.
[7] Kumar V, German MD, Shih F. An engineering approach for elastic plastic fracture analysis. NP-1931, Project 1237-1, Topical Report, EPRI, 1981.
[8] Ainsworth RA, Milne I, Dowling AR, Stewart AT. Assessment of the integrity of structures containing defects. CEGB Report R/H/R6, Revision 3, 1986.
[9] Drubay B et al. A French guideline for defect assessment at elevated temperature and leak before break analysis. In: Proceedings of 9th international conference on nuclear engineering, Paper 713, Nice, France April, 2001.
[10] Besson J, Foerch R. Large scale object-oriented finite element code design. Comput Meth Appl Mech Engng 1997;142:165–87.
[11] Kabiri MR, Laiarinandrasana L, Reytier M. In: Vejvoda S, editor. Proceedings of the 17th international conference on structural mechanics in reactor technology, Prague, Czech Republic, 2003.
[12] Cailletaud G, Saï K. Study of plastic/viscoplastic models with various inelastic mechanisms. Int J Plast 1995;11(8):991–1005.
[13] Piques R, Molinié E, Pineau A. Comparison between two assessment methods for defects in the creep range. Fatigue Fract Engng Mater Struct 1991;14(9):871–85.
[14] Landes JD, Begley JA. A fracture mechanics approach to creep cracking. In: Rice JR, Paris PC, editors. Mechanics of crack growth. ASTM STP 590. Philadelphia: ASTM; 1976. p. 128–48.